J. Fluid Mech. (1994), *vol.* 260, *pp.* 1–22

Numerical simulations of stratified inviscid flow over a smooth obstacle

By KEVIN G. LAMB

Department of Physics, Memorial University of Newfoundland, St. John's, Newfoundland, Canada A1B 3X7

(Received 29 October 1992 and in revised form 2 July 1993)

Results of numerical simulations of the flow of a non-rotating, inviscid, Boussinesq fluid over smooth two-dimensional obstacles are described. The fluid has finite depth and a rigid lid. Far upstream of the obstacle the horizontal velocity and buoyancy frequency are uniform. Comparisons with linear theory for small-amplitude obstacles are made and the long-time behaviour is compared with steady-state Long's model solutions. Comparisons with the time-dependent results of Baines (1979) are done. For Froude numbers between $\frac{1}{2}$ and 1 the obstacle amplitude is varied in order to determine the amplitudes needed to initiate wave breaking. These results are compared with the predictions of Long's model and with the experimental results of Baines (1977) showing good agreement with the latter. It is found that wave breaking occurs for amplitudes significantly lower than Long's model predicts for a large range of Froude numbers. This is shown to be the result of the generation of large-amplitude lee waves with wavelengths longer than that of stationary lee waves, but not long enough to propagate upstream. The behaviour of these waves is coupled to the generation of both longer mode-one waves which do propagate upstream from the obstacle and to mode-two waves which propagate against the flow as they are advected downstream. It is also coupled to oscillations in the wave drag. The periods of the wave drag oscillations are compared to experimental results showing good agreement with cases for which oscillations have been observed. The behaviour of these large transient lee waves is compared with the theoretical results contained in Grimshaw & Yi (1991), showing some similarities. As the Froude number approaches 0.5 the breaking behaviour is no longer due to these large waves, with the result that wave breaking occurs much later.

1. Introduction

A theoretical understanding of the waves generated by stratified flow over a finite-amplitude obstacle is far from complete. After over half a century of study there are many laboratory observations that are largely unexplained (Baines 1977, 1979; Castro, Snyder & Baines 1990). Understanding the evolving flow field is complicated by a number of factors, including strong nonlinearities, particularly in the wave generation process, and boundary-layer phenomena.

The theoretical work to date is exclusively inviscid. A natural question to ask is whether an inviscid theory is capable of explaining many of the observed phenomena. In most experiments boundary-layer separation in the lee of the obstacle is observed along with a turbulent wake. This is a viscous phenomenon and its influence on the evolving flow cannot be incorporated into an inviscid theory, though some of its effects may be parameterized (e.g. the upstream-propagating disturbances predicted by

Janowitz 1981). In experiments where flow separation is not so obvious an inviscid theory may be more applicable.

In spite of the above qualifications an understanding of the role of nonlinearities, without the complications of viscosity and its ramifications, in the generation and evolution of the wave field is desirable. Toward this goal some numerical calculations of the two-dimensional flow of a non-rotating inviscid incompressible Boussinesq fluid over smooth obstacles are done here. The fluid layer is of finite depth, with depth H far upstream and downstream of the obstacle, and has a rigid lid. Far upstream of the obstacle the fluid is assumed to have uniform horizontal velocity U and uniform stratification with constant buoyancy frequency N. Model results are compared with experimental results.

Linear theory offers a good framework for discussing the problem and the model results. In a fluid of finite depth H with a rigid lid, the vertical structure of the waves can be decomposed into distinct modes with a mode-n wave having a vertical wavenumber $m_n = n\Pi/H$. Waves with horizontal wavenumber k have a horizontal phase speed

$$c = \pm \frac{N}{(k^2+m_n^2)^{\frac{1}{2}}} \tag{1.1}$$

and horizontal group velocity

$$c_g = \pm \frac{Nm_n^2}{(k^2+m_n^2)^{\frac{3}{2}}} \tag{1.2}$$

relative to the fluid. Both $|c|$ and $|c_g|$ increase monotonically to

$$c_n = N/m_n \tag{1.3}$$

in the long-wave limit $k \to 0$. The Froude number,

$$F = K^{-1} = \frac{U}{c_1} = \frac{U\Pi}{NH}, \tag{1.4}$$

is the ratio of the upstream flow speed to the maximum horizontal group velocity. If $F < 1/n$ then sufficiently long mode-n waves can propagate upstream away from the obstacle. In addition, there is a mode-n wave which is stationary with respect to the obstacle with horizontal wavenumber

$$k_n = \frac{\Pi}{H}(K^2-n^2)^{\frac{1}{2}}. \tag{1.5}$$

Because $|c_g| < |c|$ it appears downstream of the obstacle, and hence is called a stationary lee wave.

Long (1953) derived a single nonlinear equation for the streamfunction describing steady nonlinear inviscid flow over an obstacle. If the upstream fluid velocity and the density gradient are independent of height the equation linearizes (Long 1955). The resulting equation, along with its nonlinear boundary condition, is known as Long's model. Long made qualitative comparisons of model predictions with experimental observations, showing reasonable agreement; however, large-obstacle cases exhibited turbulent eddies in the obstacle lee accompanied by large upstream modifications. Implicit in the application of Long's model to problems which initially have uniform upstream flow is the assumption that upstream-propagating waves do not modify the

incoming flow. This assumption, commonly termed Long's hypothesis, has been the focus of experimental and theoretical studies (Benjamin 1970; McIntyre 1972; Baines 1977). See Long (1972) for a review of early work.

Linear theoretical studies include two approaches. The first approach, culminating in the work of McIntyre (1972), is based on the assumption of small obstacle height. It uses the small parameter $\epsilon = a\Pi/H$ where a is the amplitude of the obstacle. The second approach uses a momentum source to represent the obstacle. Janowitz (1981) used this method to calculate steady flows. There are significant differences between the predictions of these two models. The first method predicts an $O(\epsilon)$ wave train propagating upstream from the obstacle. At a given position x the wave amplitude decays with time. In contrast, Janowitz's theory predicts a modification of the upstream flow through the generation of large upstream-propagating columnar disturbances (waves with $k = 0$). McIntyre predicted $O(\epsilon^2)$ columnar disturbances (also found by Benjamin 1970) created by nonlinear interactions in the tails of the lee-wave train. They propagate upstream only if $F < \frac{1}{4}$, suggesting that Long's hypothesis is valid for $\frac{1}{4} < F < \frac{1}{2}$.

Towing-tank experiments indicate that Janowitz's theory is valid if there is turbulent mixing in the lee of the obstacle (e.g. Wei, Kao & Pao 1975; Castro & Snyder 1988; Castro *et al.* 1990. See also Baines 1994). Baines compared experimental results with the predictions of Long's model (Baines 1977) and with those of McIntyre's theory (Baines 1979). He found that the predictions of Long's model were in poor agreement with his experimental results. He attributed this to the invalidity of Long's hypothesis. Experiments using large triangular obstacles were done by Boyer & Tao (1987) who focused on the lee-wave field, including its temporal development. They investigated the effects of obstacle height and width, showing that narrower obstacles result in larger lee waves.

The only numerical simulations of stratified flow past a smooth obstacle that have been done to date are the near-resonant ($F \approx 1$) calculations of Hanazaki (1992) who used a Navier–Stokes model with a free-slip boundary condition. Hanazaki (1989) (see also Hanazaki 1993) considered the flow of a viscous incompressible Boussinesq fluid past a thin vertical flat plate. The Reynolds numbers in his calculations were about 20 based on obstacle height, significantly lower than typical experimental values of about 200–3000 (Boyer & Tao 1987). Castro (1994) computed steady-state solutions of the same equations for a similar obstacle. He obtained solutions with Reynolds numbers as high as 200. These viscous simulations are for situations involving separated turbulent wakes, a very different situation from that considered here.

In this paper the effects of obstacle amplitude on non-resonant, inviscid flows with $\frac{1}{2} < F < 1$ are investigated. In §2 the numerical model is described. Section 3 contains the results: in §3.1 small obstacles are considered; in §3.2 the validity of Long's hypothesis is examined; wave breaking and wave drag are considered in §§3.3 and 3.4. The results are discussed and summarized in §4.

2. The numerical model

The model equations are the inviscid incompressible Boussinesq equations in two dimensions:

$$\boldsymbol{U}_t + \boldsymbol{U}\cdot\boldsymbol{\nabla}\boldsymbol{U} = -\boldsymbol{\nabla}p - \rho\boldsymbol{g} + \boldsymbol{B}(t), \tag{2.1a}$$

$$\rho_t + u\rho_x + w\rho_z = 0, \tag{2.1b}$$

$$u_x + w_z = 0. \tag{2.1c}$$

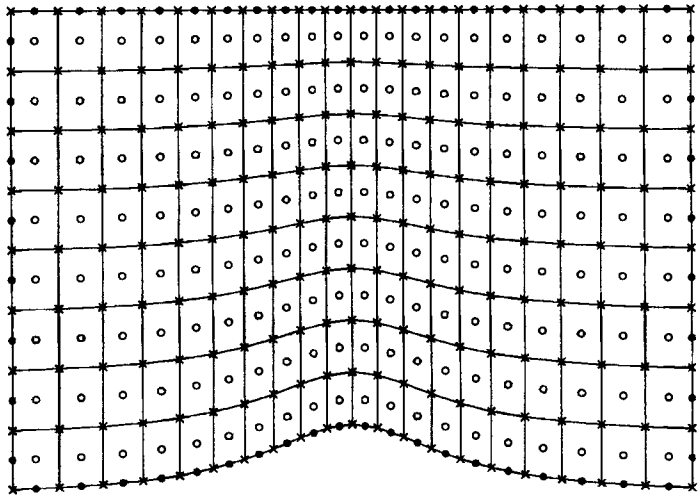

FIGURE 1. A schematic of the computational grid showing the interior and boundary vector points (open and solid circles) and the scalar vector points (×). The horizontal stretching of the grid far from the obstacle is exaggerated.

Here $\boldsymbol{U}$ is the velocity vector with horizontal and vertical components (u, w), (x, z) are the corresponding spatial coordinates, and ∇ is the gradient operator $(\partial/\partial x, \partial/\partial z)$. The fluid density is $\rho_0(1+\rho)$ and $\rho_0(gz+p)$ is the pressure (henceforth ρ and p will be called the density and pressure), $\boldsymbol{g}$ is the vector $(0, g)$ where g is the gravitational acceleration and $\boldsymbol{B}(t) = (BX(t), 0)$ is a forcing term used to accelerate the flow from rest.

The equations are non-dimensionalized using the far-upstream velocity U as the velocity scale, the fluid depth H far from the obstacle as the lengthscale, and the convective timescale H/U. The equations are solved on a domain bounded below by the topography at $z = h(x)$ and above by a rigid lid at $z = 1$. The inviscid boundary conditions are no normal flow at the upper and lower boundaries and inflow and outflow conditions at the left and right edges of the domain.

The numerical method used is the second-order projection method originally developed for a homogeneous fluid by Bell, Colella & Glaz (1989*a*). This method is second order in both time and space, and Bell & Marcus (1992) extended it to a fully stratified fluid. The method can be used on structured quadrilateral grids (Bell, Solomon & Szymczak 1989*b*). The reader should consult these papers for details on the method and on the inflow and outflow boundary conditions. The preconditioned conjugate gradient routine used by Bell *et al.* (1989*a*) for the projection was found to be too slow on the grid used here (possibly because of the high aspect ratio of the grid cells). A standard tridiagonal block matrix solver (see Golub & Van Loan 1989) was used instead.

In the present case the quadrilateral grid is constructed using terrain-following coordinates with higher horizontal resolution in a neighbourhood of the obstacle (figure 1). The outflow boundary condition used by Bell & Marcus (1992) did not work well. The domain was taken sufficiently large so that waves generated at the downstream boundary did not enter the region of interest. No waves hit the upstream boundary. Typical calculations have $I = 600$ and $M = 40$ grid cells in the horizontal and vertical respectively in the subregion $-20 \leqslant x \leqslant 20$ with Δx increasing by a factor of about 5 between the obstacle crest and $x = \pm 20$. Higher resolution runs with $I = 1200$ and $M = 50$ in this subregion were also done.

For most of the simulations discussed here the obstacle is a smooth Witch of Agnesi profile given by

$$z = h(x) = \frac{a}{1+(x/D)^2}. \tag{2.2}$$

In this case the only free parameters in the problem are the obstacle amplitude a, the width of the obstacle specified by the half-width D and the Froude number F.

The flow is smoothly accelerated from 0 to 1 at the inflow boundary by using the horizontal forcing

$$BX(t) = \begin{cases} (1/FT)(1-\cos(2\Pi t/FT)), & 0 \leqslant t \leqslant FT; \\ 0, & t \geqslant FT. \end{cases} \tag{2.3}$$

A fast startup was used with a forcing time $FT = 0.01$. This mimics laboratory experiments and linear theory which assume an impulsive startup. Tests with $FT = 0.0005$ gave virtually identical results.

The model was tested by verifying that the flow initialized with steady flow solutions provided by Long's model, obtained numerically (Davis 1969), remained steady. Further tests included running the model from a state of rest with $F = 1.5$ for a variety of obstacle amplitudes ($\leqslant 0.25$) and widths. Steady states over the obstacle were achieved by $t \approx 10$. The horizontal velocity profiles above the obstacle crest agreed with those given by Long's model. Further evidence that the model is working correctly is provided in §3.1 where it is shown that as $a \to 0$ the evolving wave field converges to the time-dependent linear solution.

3. Results

3.1. *Small-amplitude results*

The horizontal velocity can be decomposed as

$$U_1 = \frac{1}{1-h(x)} + \sum_{n=1}^{\infty} aU_n(x,t)\cos\left(n\Pi\frac{z-h(x)}{1-h(x)}\right). \tag{3.1a}$$

Far from the obstacle where h is essentially zero this becomes

$$U = 1 + \sum_{n=1}^{\infty} aU_n(x,t)\cos(n\Pi z) \tag{3.1b}$$

and U_n can unambiguously be identified as a mode-n wave. In the linear regime U_n is independent of a. In figure 2 numerical results using a Witch of Agnesi profile for $K = 1.5$ and $D = 1.6$ are compared with the linear solution for different obstacle amplitudes a. Linear transient solutions were numerically calculated following Baines (1979) (note that his equation A 8 needs to be multiplied by $\pm$ with corresponding changes in A 13). The model results show that linear theory is accurate only if the obstacle amplitude is extremely small, i.e. below about 0.01 in this case. As a increases the amplitude of U_n increases. When $a = 0.05$ both the wave amplitudes and wavelengths are larger than linear theory predicts. This leads to a small delay in the arrival of the wave crests, but not in the arrival of the wave front. This may be a result of the fact that as the obstacle amplitude increases the Froude number over the obstacle increases, resulting in energy escaping from the vicinity of the obstacle more

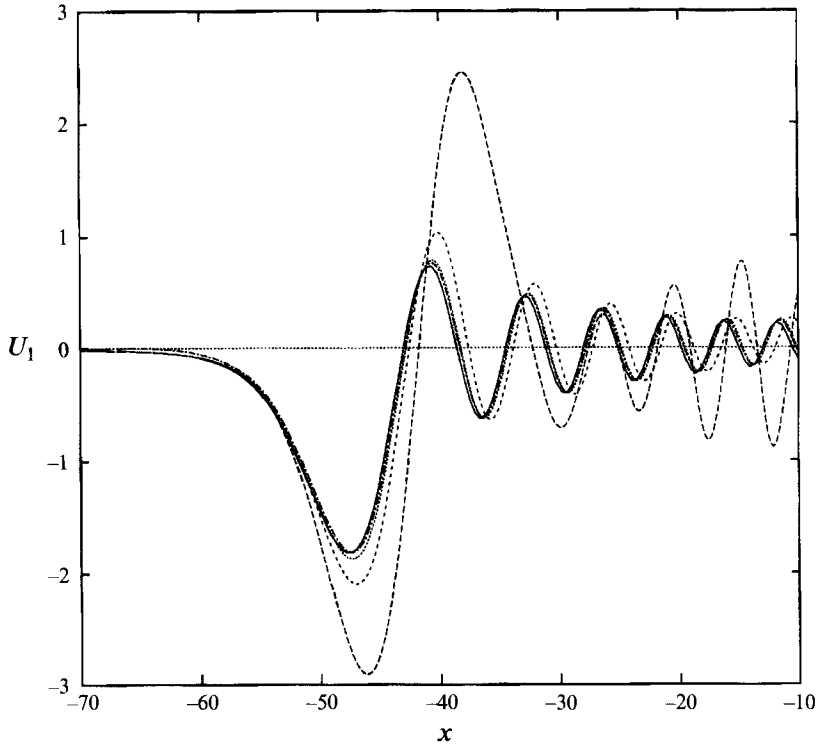

FIGURE 2. Mode-one horizontal velocities $U_1(x, t)$ upstream of the obstacle (Witch of Agnesi) at time $t = 100$ for different amplitudes a are compared with linear theory showing good agreement for a less than about 0.01. A qualitative difference from linear theory (solid line) occurs for $a = 0.13$. Here $K = 1.5$ and $D = 1.6$. Amplitudes are for $a = 0.13$ (———), $a = 0.05$ (– – – –), $a = 0.01$, (· · · · ·), $a = 0.002$ (— · — · —).

slowly. For a much larger obstacle ($a = 0.13$) this trend continues but there is now a striking qualitative difference as well. A very large leading wave is followed by much smaller waves which are growing in amplitude. Figure 3 shows U_1 for the $a = 0.13$ case after a much longer time. The single large leading wave has evolved into several waves of decreasing amplitude. This appears to be a dispersive phenomenon. Following is a series of wave packets of much smaller amplitude.

The propagation speed of the leading wave was determined by following the first maximum of U_1. This lead wave initially has an upstream propagation speed of about 0.42 which increases to about 0.49 by $t = 80$ and to about 0.495 by $t = 400$, close to the linear long-wave value of 0.5. The initial propagation speed is about 5% less than the linear long-wave speed relative to the water. For different obstacles Baines (1979) observed values about 10% less.

Baines (1979) did a number of experiments designed to investigate the efficacy of linear theory. His comparisons with linear theory showed striking differences. Some model runs using Baines' obstacle M2 were done in order to see if these differences could be attributed to nonlinearities (Baines did not observe any lee-wave separation in his experiments with this obstacle). Obstacle M2 was 1.1 cm high and 55 cm long with a flat top tapered in the last 3 cm on each end (the model results were insensitive to how it is tapered down). The non-dimensional obstacle height is 0.059. Its profile is shown in figure 4.

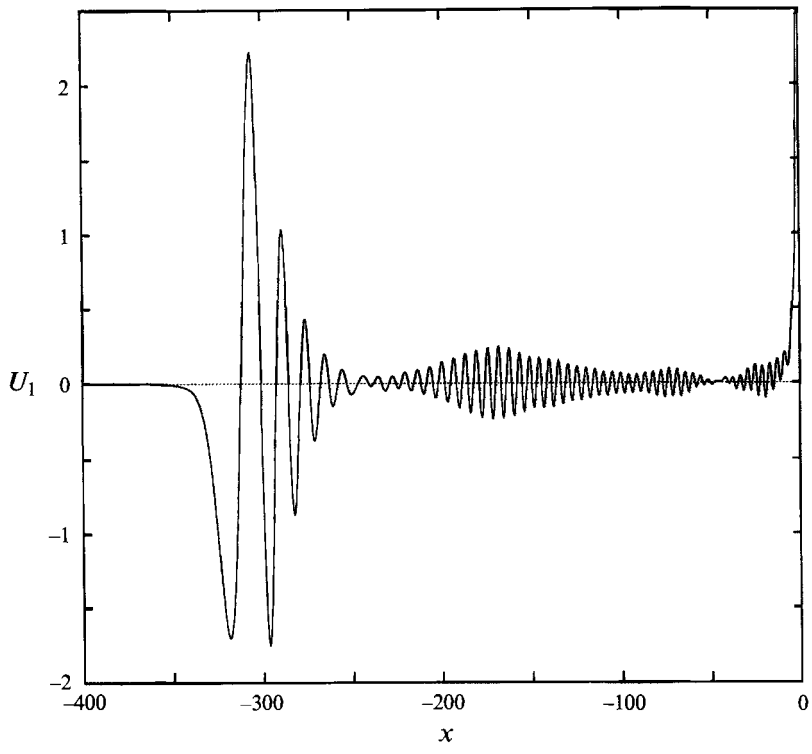

FIGURE 3. Mode-one horizontal velocity $U_1(x, t)$ upstream of the obstacle at $t = 650$ for a large-amplitude obstacle (below the breaking height). Same obstacle ($a = 0.13$) and value of K as in figure 2.

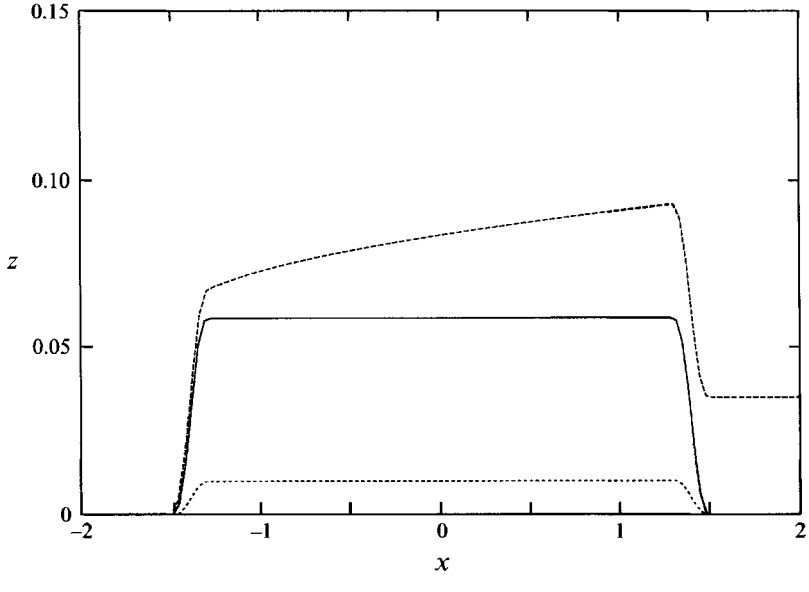

FIGURE 4. Obstacle profiles. The solid curve is obstacle M2, $a = 0.059$. Also shown is the profile modified by adding a boundary layer for the case $K = 1.59$, $a = 0.059$ (————), as well as a scaled-down obstacle used to find the linear response, $a = 0.01$ (------).

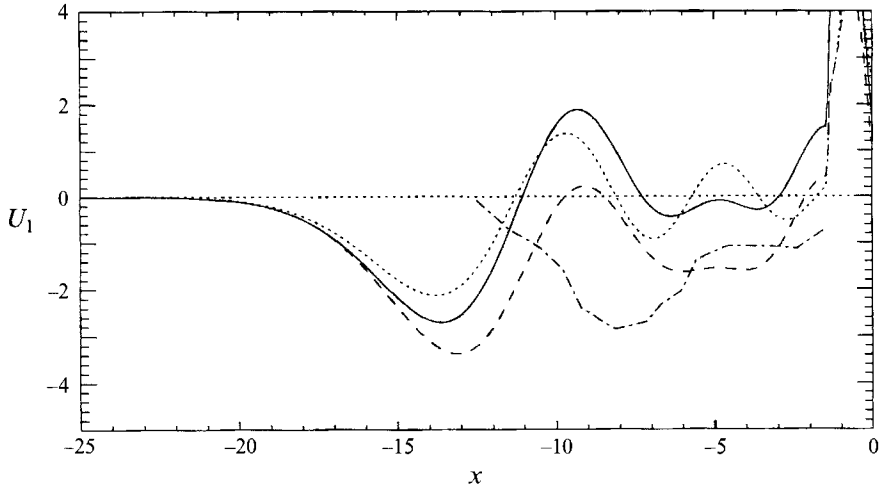

FIGURE 5. Mode-one horizontal velocity $U_1(x, t)$ upstream of obstacle M2 at $t = 26.42$ for $K = 1.59$ (——). The obstacle lies between $x = -1.475$ and $x = 1.475$. For the case with a boundary layer added to the profile (— — — —) the obstacle height is taken as its height at the midpoint (= 0.0836) following Baines (1979). Small obstacle results with $a = 0.01$ (------) and Baines data (– · – · –) are also shown.

Figure 5 shows U_1 upstream of the obstacle for the case $K = 1.59$ at $t = 26.42$, the same time as Baines reports measurements for. Baines' measurements, appropriately scaled, are included as well as model results for a similar obstacle with an amplitude of 0.01. The latter is expected to be a good approximation to the linear solution. The leading depression in U_1 is very similar in size and width to that in the observations, however its position agrees with the predictions of linear theory and is well ahead of the experimentally observed wave front. U_1 then briefly changes sign, in contrast to the observations, before attaining a relatively constant negative value between $x = -7$ and $x = -3$. In the observations a flat region of similar length is seen at approximately the same location with a value about four times as large.

As pointed out in Baines (1979), the thickness of the boundary layer on this obstacle is very significant, about 30–35% of the obstacle height at the obstacle midpoint. Some model runs were done using an obstacle profile modified by adding a boundary layer. The formula for the thickness of a steady-state boundary layer on a flat plate is used as an approximation. The new profile is given by

$$h(x) = h_{M2}(x) + 1.72(\nu(x - x_l))^{\frac{1}{2}} \tag{3.2}$$

for $x_l \leqslant x \leqslant x_r$, where x_l and x_r are the left and right edges of the obstacle and $h_{M2}(x)$ is the obstacle profile. Behind the obstacle the new profile is given by

$$h(x) = 1.72(\nu(x_r - x_l))^{\frac{1}{2}}. \tag{3.3}$$

That is, the boundary layer is assumed to stop growing and remain constant in thickness downstream of the obstacle. In the experiments the boundary-layer thickness would have decreased as the fluid flowing off the back of the obstacle was accelerated because of the bottom boundary condition (the obstacle was towed along the bottom of the tank). In general, boundary-layer separation or thickening could occur under lee-wave crests due to adverse pressure gradients and reduced flow speeds. This may

effectively extend the boundary-layer wake in the downstream direction. In Baines' experiment the buoyancy frequency was $N = 1.05\ \mathrm{s}^{-1}$ (personal communication) so that for $K = 1.59$ the value of the non-dimensional viscosity ν is about 0.000139. This corresponds to a Reynolds number, based on the obstacle height, of about 428. The modified profile is included in figure 4.

The results obtained using this modified profile are included in figure 5. Following Baines (1979), the value of a used in (3.1a) is the height of the obstacle plus the boundary-layer thickness at the midpoint $x = 0$. In this case this sum is 0.0836 (it varies with K). The most noticeable modification to the upstream profile of U_1 is that it has been shifted down. This is due to the upstream-propagating columnar disturbance generated by the permanent change in fluid depth downstream of the obstacle. In experiments in which the obstacle is towed along the bottom of a tank the boundary layer, as discussed above, will get thinner, possibly negating the columnar disturbance. If the obstacle is towed along the top of the tank the thinning of the wake will take much longer so that experimental results obtained with surface- or bottom-mounted obstacles could differ. The flat part of curve centred at $x \approx -5$ is now comparable in magnitude to the corresponding feature in the experiments. It is a transient phenomenon.

Comparisons with Baines' results for other values of K were also made, showing similar agreements and differences. In all cases, the vertical profile of the horizontal velocity above the obstacle more closely resembled the linear solutions shown by Baines (1979) than they did the experimental values.

3.2. *Long's hypothesis*

Baines (1977) concluded that Long's hypothesis is invalid because upstream columnar disturbances are generated. These conclusions were based on the large discrepancies between predicted and observed horizontal velocity profiles above the crest of the obstacle. An unanswered question is the cause of the upstream-propagating disturbances. Were they due to nonlinear effects as suggested by Castro *et al.* (1990) or viscous effects (including flow separation)? Baines (1977) did not observe a wake in his experiments.

In order to test the possibility that the invalidity of Long's hypothesis is due to nonlinear effects one very long time run was done. Figure 3 shows $U_1(x, t)$ at $t = 650$ for $K = F^{-1} = 1.5$ obtained using a Witch of Agnesi obstacle with a half-width $D = 1.6$ and an amplitude $a = 0.13$. The amplitudes aU_1 of the waves just upstream are extremely small, being below 0.013 within a distance of 120 of the obstacle. The wave amplitudes do not appear to be decaying. The horizontal velocity profiles through a vertical line above the obstacle crest oscillate in time about the Long's model solution (figure 6). These small oscillations do not appear to be decaying with time.

The numerical results suggest two things for inviscid flows. First, a steady state is achieved only after a very long time, if ever. Second, Long's hypothesis is valid in the sense that after an initial transient period the flow field exhibits very small oscillations about Long's model solution.

The model results should be contrasted with the experimental observations of Baines (1977). Using a much narrower Witch of Agnesi obstacle ($D \approx 0.19$) with similar amplitude ($a = 0.12$) he found poor agreement with Long's model. The elapsed time between the start of the experiments and the observations is not given. Taking the stated typical fluid depth of 0.3 m, total density difference of 0.4%, and upper bound on the towing times of 200 s, the non-dimensional towing time is about 15 for $K = 1.5$. The largest upstream-propagating wave in the numerical calculation (the peak of just

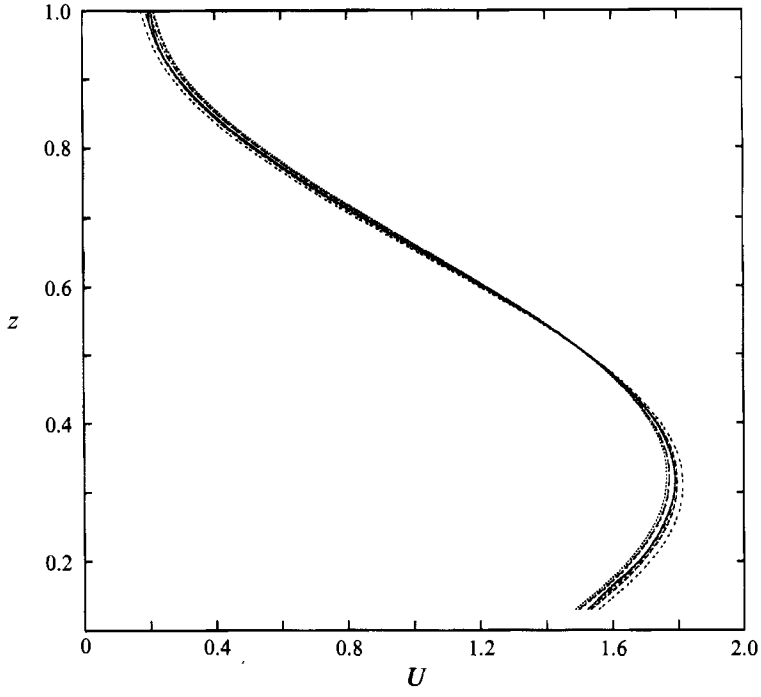

FIGURE 6. Horizontal velocity profiles above the obstacle crest at various times are compared with Long's model solution. Obstacle and value of K as in figure 3. At the bottom of the plot the curves, going from left to right, are for $t = 620$, 630, 610, 640, 600 and 650. Order is reversed at top. Superimposed (solid curve) is Long's model solution which is almost identical to the model result at $t = 640$.

under 2.5 in figure 3) is generated at a non-dimensional time of about 30. This suggests that a steady state may not have been achieved. Alternatively, viscosity could account for the generation of upstream-propagating disturbances in one of two ways: flow separation in the lee of the obstacle with a wake too small to be seen, or through an effective change in fluid depth due to a boundary layer as discussed in §3.1.

3.3. *Wave breaking*

Baines (1977) compared the occurrence of wave breaking (overturning), transient or otherwise, in his experiments with the predictions of Long's model. Using smooth Witch of Agnesi obstacles he found that wave breaking usually occurred at obstacle amplitudes well below the breaking amplitude predicted by Long's model for $F < 1$. The exception was for $K = F^{-1}$ very close integer values. In those cases breaking was not observed, even at amplitudes well above the breaking value given by Long's model. A series of calculations were done in order to investigate this for $\frac{1}{2} < F < 1$.

As the obstacle amplitude a is increased from small values a critical amplitude a_b is reached above which waves break; a_b depends on the Froude number F and on the obstacle width D. The breaking amplitude a_{bL} predicted by Long's model is quite sensitive to D when D is small. For example, for $F = 0.826$, a_{bL} has values of 0.196 and 0.145 for $D = 0.095$ and 0.20 respectively. In Baines experiments D ranged between 0.13 and 0.3. Values for the individual data points shown by Baines (his figure 1) are not given.

Figure 7 shows a_{bL} as a function of F for $D = 0.17$. The hydrostatic breaking

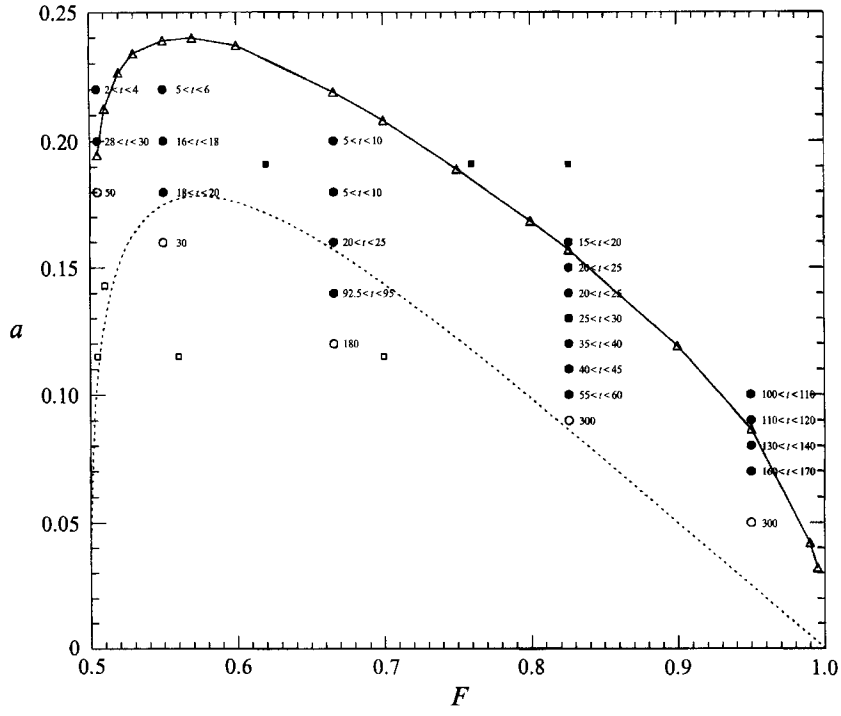

FIGURE 7. Breaking results for Witch of Agnesi obstacles. The triangles connected by the solid curve are breaking amplitudes predicted by Long's model for $D = 0.17$ computed to within ± 0.001. The dashed curve is the breaking amplitude given by the hydrostatic Long's model. Solid circles represent model runs for which breaking waves were observed, with the breaking time t indicated. Open circles represent cases for which breaking waves were not observed, with the model run time indicated. Baines (1977) experimental results are included, with solid/open squares for breaking/non-breaking cases. In the model runs $D = 0.17$ while in the experimental results D varied between 0.13 and 0.3. Model runs are for $F = 0.505$, 0.55, 0.666, 0.826 and 0.95.

amplitude determined using the hydrostatic Long's model (Long 1955) is included (dashed curve). Numerical results for $D = 0.17$ are also shown. Solid/open circles represent breaking/non-breaking cases. Also shown are Baines' results (squares): all the breaking cases (solid squares) lie above the hydrostatic breaking amplitude curve while all the non-breaking cases (open squares) are below it or are close to $F = 0.5$. Baines' results should not be compared to the solid curve as the obstacle widths differ.

The general pattern of the numerical results concur with the experimental results of Baines (1977). Breaking occurs for a well under a_{bL} except when F is close to 0.5. In addition note that breaking occurs if the obstacle amplitude is above the hydrostatic breaking amplitude except for $F \approx 0.5$ (and possibly 1). The predicted dip in the breaking amplitude near $F = 0.5$ does not seem to occur.

The reason for the rapid onset of breaking is due to the same mechanism for all cases with $F \gtrsim 0.55$. As an example consider $F = 0.826$. Breaking occurred in distinct locations in an ordered manner. Each of these separate occurrences will be called a breaking event. Increasing the resolution changed the details of the flow after the first occurrence of breaking. The qualitative features, including the locations and times of the breaking events, were unchanged.

Model simulations give a breaking amplitude a_b between 0.09 and 0.10 whereas $a_{bL} = 0.157$. The hydrostatic breaking amplitude is 0.086. For values of $a \geqslant 0.15$ the

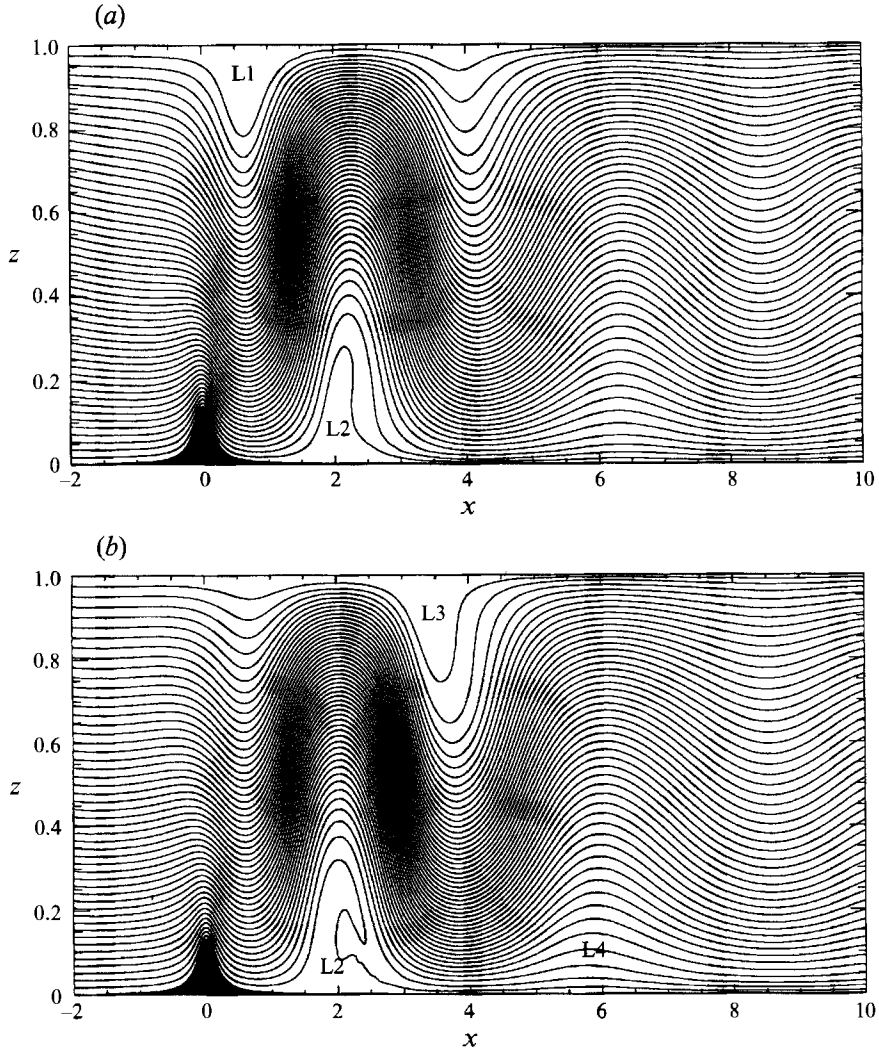

FIGURE 8. Density contours for the case $(a, F, D) = (0.13, 0.826, 0.17)$. High-resolution run (see §2). (*a*) $t = 35$, (*b*) $t = 40$.

first strong breaking event occurs near the upper boundary in the centre of the first trough of the isopycnals just downstream of the obstacle (location L1, see figure 8). For $a = 0.15$ overturning begins at $t \approx 20$ and is well developed by $t = 25$. A second breaking event starts at $t \approx 30$. This time it is at the bottom boundary under a large crest (location L2). This result is typical of cases with $a \geqslant 0.15$. As a is increased the overturning occurs earlier, becomes stronger and the first event becomes more dominant. As a decreases, the strength of the first overturning event at L1 decreases considerably. The second breaking event at L2 becomes stronger. Figure 8 shows a series of density contour plots for $a = 0.13$. Between $t = 25$ and 30 weak short-lived overturning occurs at location L1. At $t = 35$ overturning has started at location L2. It is well developed by $t = 40$ at which time overturning is just about to occur near the top of the domain in the second trough (location L3). At $t = 45$ the overturning region at L2 has collapsed while that at L3 is well developed. By $t = 50$ there is again strong

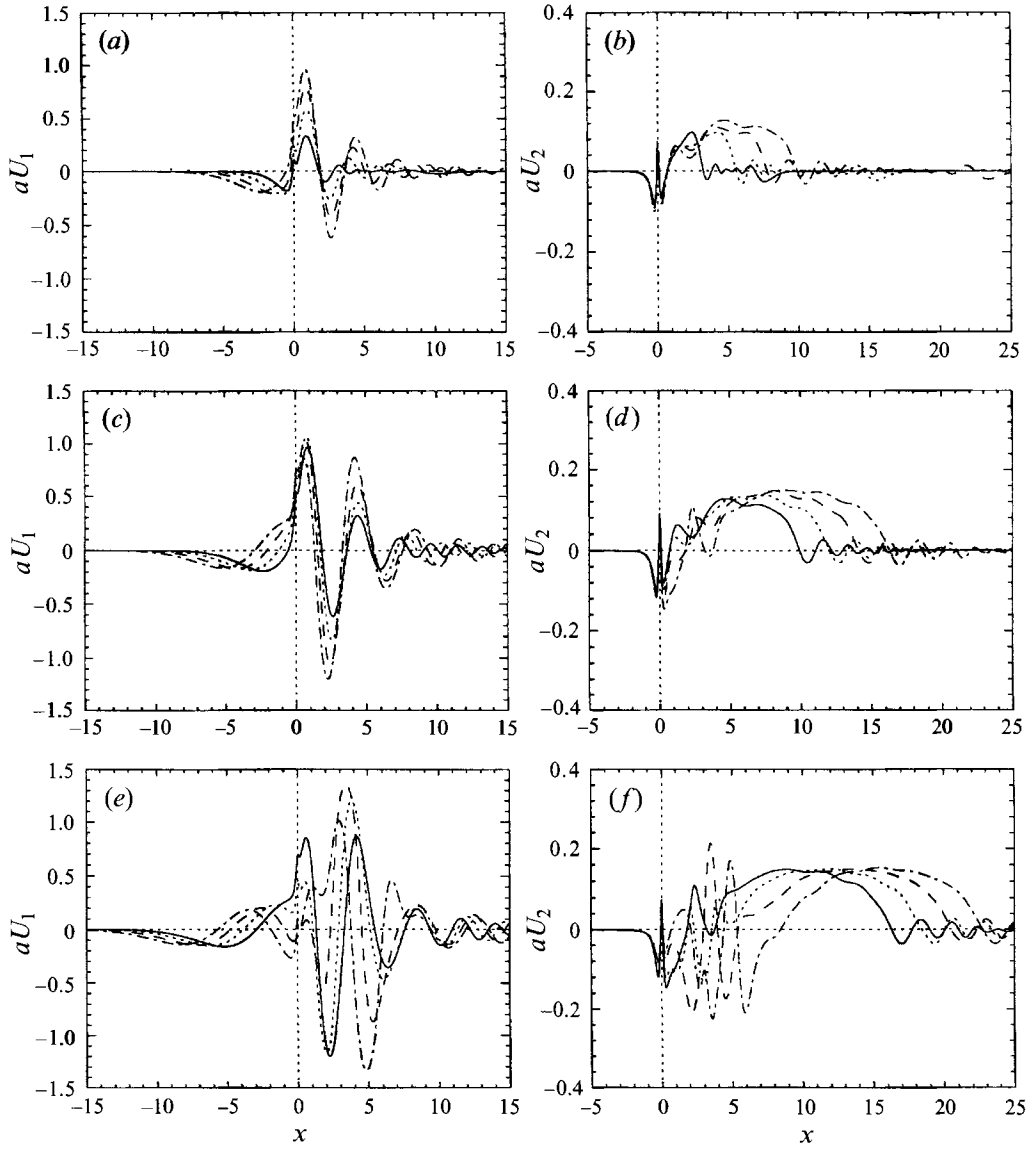

FIGURE 9. Plots of $aU_1(x,t)$ (*a*, *c* and *e*) and $aU_2(x,t)$ (*b*, *d* and *f*) at various times for the case $(a,F,D) = (0.13, 0.826, 0.17)$. Curves ——, · · · ·, ----, – · – · – · – are for times $t = 5$, 10, 15, and 20 respectively in (*a*) and (*b*); $t = 20$, 25, 30, 35 in (*c*) and (*d*); and for $t = 35$, 40, 45, and 50 in (*e*) and (*f*).

overturning near the bottom, now in the second crest (location L4). As a is decreased still further, the strength of the strongest breaking event decreases and the position of the first breaking event moves downstream. The result is that for $a = 0.10$ the first breaking event occurs at about $t = 60$ at location L4 (in this case at $x \approx 7$).

Plots of aU_1 and aU_2 for various times are shown in figure 9 for the case $a = 0.13$. Plots are very similar for the case $a = 0.10$, which did not break until $t > 55$. The amplitudes of the higher-mode waves are much smaller. Recall that the identification of U_n with a mode-n wave becomes invalid close to the obstacle. For $a = 0.13$ the slope

of the obstacle has a magnitude slightly less than 0.01 at $x = \pm 0.9$, so this identification is quite good at this distance. The obstacle has its maximum slope at $\pm D/3^{\frac{1}{2}} \approx \pm 0.1$. The small sharp peak-dip seen in the figures is centred at this location.

A large mode-one wave is seen to develop just downstream of the obstacle. Since the contribution to the horizontal velocity from a mode-one wave is $aU_1 \cos(\Pi z)$, overturning occurs near the top when aU_1 becomes larger than 1 and near the bottom when aU_1 becomes less than -1. The value of aU_1 exceeds 1 by $t = 0.25$ at $x \approx 0.75$. After this, the wave grows slightly and then dramatically decreases in amplitude in conjunction with a large-amplitude wave of positive U_1 leaving the obstacle to propagate upstream. After the mode-one lee wave collapses, it grows again and then collapses as a second mode-one wave leaves the obstacle to propagate upstream. Every time the mode-one lee wave grows renewed breaking is possible.

The minimum of U_1 at $x \approx 2.2$ (location L2) also grows rapidly, dipping to -1.2 at $t = 35$. Note the stronger breaking seen in figure 8(*b*) at this location. After $t = 40$ the amplitude suddenly decreases in magnitude while the amplitudes of the next maximum and minimum of U_1 grow rapidly, leading to overturning in locations L3 and L4. This case was only run until $t = 50$. It appears that breaking will occur farther and farther downstream at later times.

The large-amplitude mode-one waves downstream of the obstacle have a slight upstream phase velocity. This can be explained using linear theory. The wavelength of the stationary lee waves is $\lambda_l = 2.93$. The horizontal group velocity relative to the obstacle is negative only if the wavelength is greater than about 5.42. The peak-to-peak distance of the large waves just downstream of the obstacle varies somewhat but is always larger than λ_l. For the $a = 0.10$ case (non-breaking for $t < 50$), the distances between the first and second peaks in U_1 are about 3.34, 3.4, 3.32 and 3.13 for $t = 20$, 25, 30 and 35 respectively. Thus, linear theory predicts that these waves have negative phase velocities and positive group velocities, as is observed. Taking $\lambda = 3.34$ as a representative case the group velocity is 0.24, a value in good agreement with what one would estimate from figure 9. Lee waves with wavelengths larger than the wavelength of stationary lee waves predicted by linear theory were observed by Boyer & Tao (1987) in their experiments.

A long mode-two wave of positive amplitude develops downstream of the obstacle (figure 9). Its propagation speed downstream is that of a long mode-two wave propagating against the flow. It will slightly weaken the breaking in the top and bottom quarters of the domain and enhance it in the middle half. An examination of the mode-two waves over longer times shows that a depression in U_2 leaves the obstacle at the same time as an upstream-propagating elevation of U_1 does. Figure 10 shows U_1, U_2 and U_3 at $t = 50$ for the case $(K, a) = (1.5, 0.12)$. The large positive values of U_1 just downstream of the obstacle has collapsed for the fourth time. Four large mode-two waves can be seen downstream of the obstacle with the fourth depression just leaving it. Four elevations of U_1 can be seen upstream of the obstacle. A similar pattern in U_3 is not apparent.

Movies of the evolving waves have been made which clearly show a lee wave attached to the downstream side of the obstacle. This lee wave has an oscillating amplitude. Waves farther downstream with an upstream phase velocity do not always propagate all the way up to the obstacle, although they can propagate a considerable distance upstream before losing their identity. The amplitude of the oscillation of the lee wave attached to the obstacle may increase with time. This happens for the case shown in figure 10 as can be deduced from the growing amplitude of the upstream-propagating waves. This is why breaking occurred after such a long time when $(K, a) =$

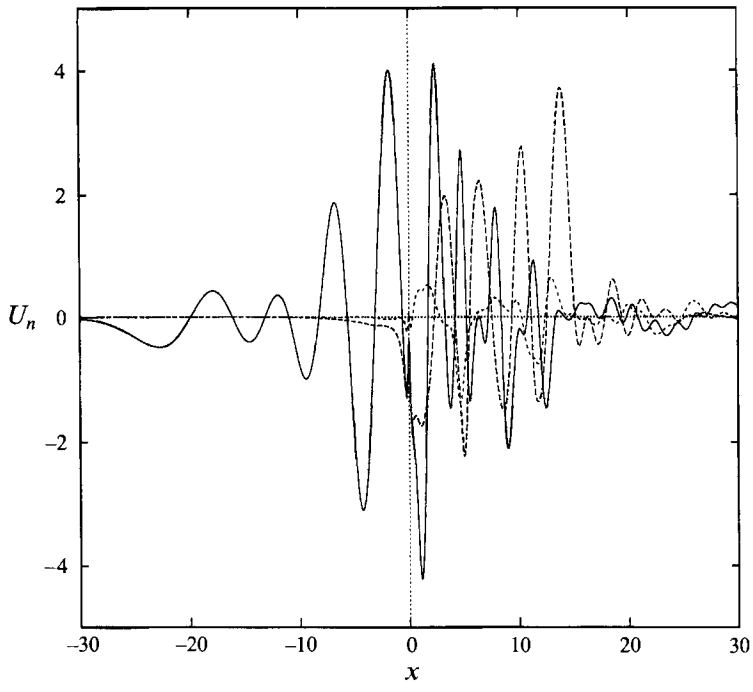

FIGURE 10. U_1 (——), U_2 (— — —) and U_3 (– – – –) at $t = 50$ for the case $(K, a) = (1.5, 0.12)$ and $D = 0.17$. The four oscillations of U_1 upstream of the obstacle (at $x = 0$) match with four large oscillations in U_2 downstream of the obstacle. The large positive value of U_1 immediately downstream of the obstacle has just collapsed. Coupled to this, a large mode-one wave (positive U_1) has just left the obstacle to propagate upstream and a depression in U_2, propagating against the flow, has just left the obstacle and is being advected downstream.

(1.5, 0.14). In this case the eighth oscillation of the lee wave was large enough to break. For $(K, a) = (1.5, 0.16)$ breaking occurred the second time this lee wave grew in amplitude. For the case $(K, a) = (1.5, 0.12)$ this growth had stopped and was decreasing by $t = 180$. It seems that breaking would never occur for this case. Note the difference between these cases and the case shown in figure 3 which has the same Froude number and a similar amplitude but a much wider obstacle. This indicates that the obstacle width is an important parameter. For the case with $(F, a) = (0.826, 0.09)$ breaking had not occurred by $t = 300$. The amplitude of the oscillations of the attached lee wave was still growing, hence breaking could have eventually occurred.

The hydrostatic breaking curve appears to be an approximate boundary separating the region where breaking occurs during the first growth of the lee wave attached to the obstacle from the region where breaking first occurs in subsequent oscillations of this lee wave. Exceptions to this are for F close to 0.5 or to 1. The apparent significance of the hydrostatic breaking amplitude for the obstacle width used in these model runs may be coincidental.

The coupling of the mode-one and mode-two waves leaving the obstacle suggests a nonlinear mechanism, possibly with interaction with the obstacle, self-interaction of the mode-one wave, and interaction between the mode-one and mode-two waves. A partial theoretical explanation for the generation of these large-amplitude waves may be provided by the work of Grimshaw & Yi (1991) (henceforth GY). They derived an evolution equation for the flow of a weakly stratified fluid over an obstacle when the flow is near resonance (that is, $F \approx 1$). In their figure 10 two cases in the Boussinesq

limit are shown. Large waves with negative phase speeds are seen downstream of the obstacle. In one case they break and in the other they do not. As pointed out by Baines (1994), the difference between these two cases can be characterized by the value of $P = (F-1)/a$. Using equations (2.15*b*), (3.1) (3.5*a*) and (4.2) of GY we find that for the breaking case $P = -4/\Pi \approx -1.27$ while for the non-breaking case $P = -12.5/\Pi \approx -3.98$. In the limit $F \to 1^-$ the hydrostatic breaking curve is asymptotic to the straight line $a = \frac{1}{2}(1-F)$. Thus, in the breaking case a lies above the hydrostatic breaking curve, while in the non-breaking case a is below it.

In the breaking case shown in GY breaking occurs quickly, before the first upstream-propagating wave has left the obstacle. Extrapolating along the line $P = -1.27$ we find that, for $F = 0.826$, a is 0.137. For an amplitude of 0.14 the numerical results show that strong breaking first occurs immediately downstream of the obstacle, just as in GY, between $t = 20$ and 25. The non-dimensional breaking time of 7.7 reported in GY is equal to about 5 of the model time units for this case. The obstacle used in GY was, however, much wider and had a different shape than the obstacles used in the above model runs. Some model runs were done using the same obstacles as used by GY. This obstacle is given by

$$h(x) = a \exp(-0.09\alpha x^2). \tag{3.4}$$

When $F = 0.826$, $\alpha \approx 8.59$. In this case breaking first occurred between $t = 13$ and 14, almost three times later than the breaking time given by GY. When $F = 0.95$ we have $\alpha \approx 2.47$ and $a \approx 0.04$. Breaking now occurred at a time between $t = 80$ and 84. This is slightly more than twice the breaking time given in GY, which is about 37 model time units. Thus, the breaking time in the model runs is about two or three times larger than the time given by Grimshaw & Yi's equation, with better agreement closer to resonance.

In the non-breaking case shown in figure 10 of GY, three waves can be seen propagating upstream from the obstacle. The first and second appear to leave the obstacle in conjunction with a large wave collapsing just downstream of the obstacle, as in the numerical results. After the second of these has collapsed the waves immediately downstream of the obstacle are much smaller in size and appear to be stationary.

The theoretical results of GY do not involve nonlinear interactions between modes and hence do not provide an explanation for the generation of the mode-two waves. The mode-two wave has a positive horizontal velocity at the top of the domain and hence inhibits overturning. This may partly account for the longer breaking times in the model. The theory also does not explain why the oscillations of the lee wave attached to the downstream side of the obstacle may grow in amplitude in some cases.

The above discussion of the evolving wave field is applicable for F between about 0.55 and 1. As F increases to 1 the upstream group velocity goes to zero and the wave field evolves on a slower timescale resulting in increased breaking times. Because of the extremely slow evolution of the wave field for $F = 0.95$ it is difficult to look at this case in as much detail as for the smaller F values. In this case breaking was observed only after very long times at location L1. For $F = 0.55$ the breaking occurring for $a = 0.2$ and 0.18 is unusual. It occurs slightly below the middle of the domain at $x \approx 4$ where a mode-one wave and mode-two wave combine to produce overturning. $F = 0.55$ appears to be in a transition region between the different behaviour that occurs for smaller and larger values of F.

The evolution of the flow is very different when $F = 0.505$. This is well illustrated by the case with $a = 0.2 > a_{bL} = 0.1945$. Large mode-one waves downstream of the obstacle are no longer present. Breaking occurs at $t \approx 30$ because of a very slowly

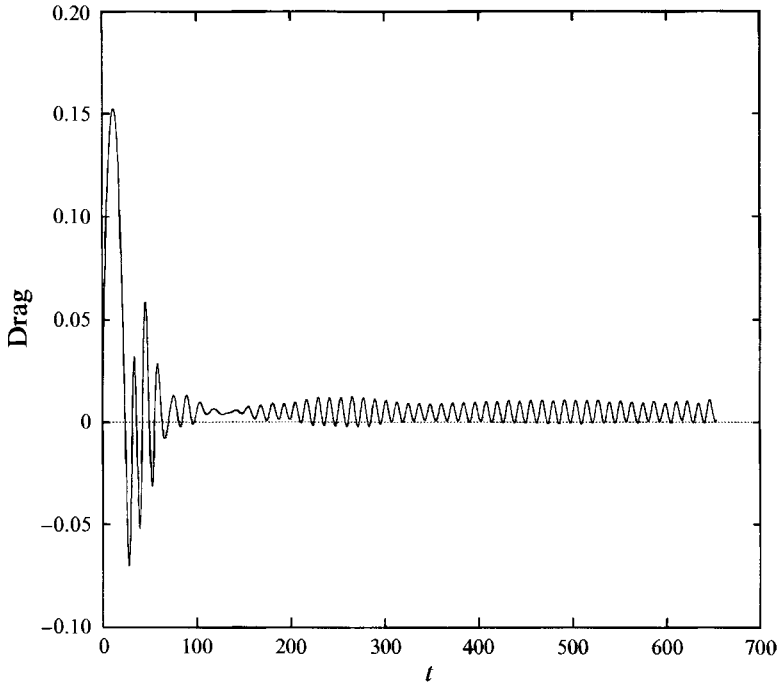

FIGURE 11. The wave drag for the long time run for which U_1 is shown in figure 3 at $t = 650$. The number of oscillations in the wave drag and in the number of wave upstream of the obstacle is the same. Note the similarity in the variation of the amplitude of the wave drag and upstream waves.

strengthening mode-two wave over the obstacle. This suggests a gradual evolution to Long's model solutions, with breaking occurring whenever $a > a_{bL}$. Because of the length of time required for breaking it was not observed by Baines (1977).

3.4. *Wave drag*

The time dependence of the wave drag ($= \int ph'(x)\,dx$) shows an oscillatory behaviour, with one oscillation for each wave that has propagated upstream from the obstacle. In figure 11 the wave drag for the long-time run shown in figure 3 is shown. A qualitative agreement between the variation in wave drag amplitude and the variation of the amplitude of the upstream waves is apparent. Wave drag is at its maximum when the fluctuating lee wave just downstream of the obstacle has its peak value of U_1.

The wave drag varies approximately periodically with time. The period is independent of the obstacle amplitude with approximately constant minimum values, slightly below zero, and with maximum and average values increasing with obstacle amplitude. The amplitude of the wave drag oscillations also appears to be independent of K for fixed a. Figure 12 shows the period of the wave drag oscillations as a function of K. As $K \to 1$ the period goes to infinity (e.g. for $K = 1.05$ the period is about 320).

Castro *et al.* (1990) did a number of towing-tank experiments with bluff obstacles. They noted that for K between 1.5 and 2.0 there were non-decaying periodic fluctuations in the measured drag on the obstacle. The measured periods varied slightly depending on the obstacle, decreasing roughly linearly from a value of about 13 at $K = 1.5$ to between 6 and 8 at $K = 2.0$. The present numerical results show a period of about 12.25 for $K = 1.5$ which decreases to about 9.75 at $K = 1.67$ after which it appears to remain steady. Thus, the agreement in the wave drag periods is quite good,

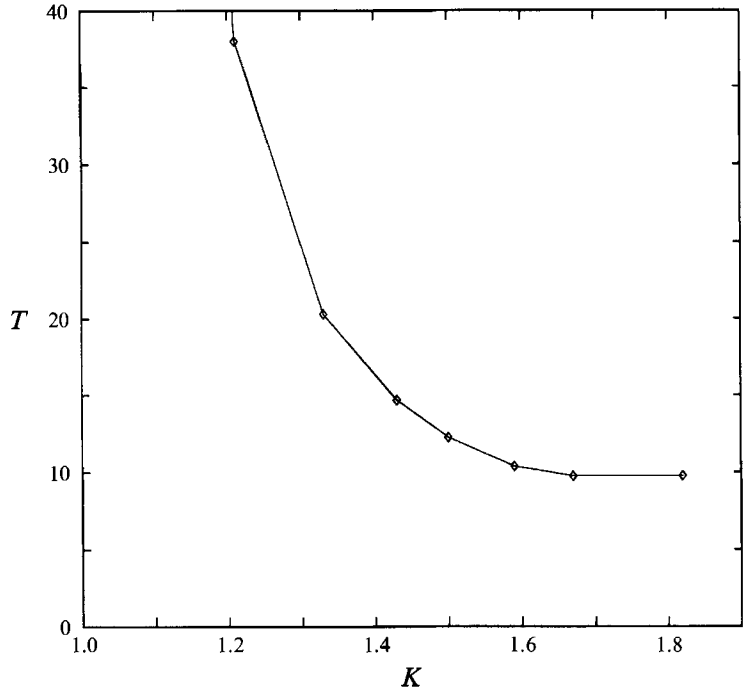

FIGURE 12. Period T of the wave drag oscillations as a function of K for $D = 0.17$. The period is independent of the obstacle amplitude.

in spite of the fact that in the experimental cases there was boundary-layer separation and a wake attached to the obstacle.

The presence of wave drag oscillations for $K < 1.5$ differs from the experimental results. It is possible that in the experiments these oscillations were damped out by the turbulent mixing. The numerical result that the oscillation period goes to infinity as $K \to 1$ is expected because as $K \to 1$ the propagation speed with respect to the obstacle decreases and the minimum wavelength of upstream-propagating waves increases. Using the long-wave propagation speed the oscillation period at a fixed point x is $\lambda/(K-1)$, where λ is the wavelength. Model results show that the oscillation period has an approximate $(K-1)^{-1}$ behaviour in the mid-range of K values. For $K \gtrsim 1.65$ the periods are independent of K. This requires $\lambda \sim K-1$ as $K \to 2$. For values less than 1.2–1.3 the model period increases more rapidly than $(K-1)^{-1}$, a result of the larger wavelengths.

4. Discussion and conclusions

The evolution of the wave field generated by flow over a smooth two-dimensional obstacle has been investigated. The fluid has a rigid lid with a depth of unity far from the obstacle. Starting from a state of rest and uniform stratification the flow was smoothly accelerated over a very short time interval to a constant uniform speed $u = 1$ far from the obstacle. The startup mimics an impulsive start. A smooth narrow Witch of Agnesi shaped obstacle with a fixed width was used for most model runs. Only Froude numbers between 0.5 and 1 have been considered.

It was found that linear theory accurately predicts the amplitude of the upstream-propagating waves only if the obstacle amplitude is very small (below 0.01 for the case

considered). As a is increased the upstream-propagating waves become larger than, and slightly lag, those predicted by linear theory. The position of the wave front agrees with linear theory for all cases run. For large-amplitude obstacles there is a significant qualitative difference in the variation of the wave amplitudes. In general, a packet of large-amplitude waves precedes much smaller amplitude waves. The wave amplitude does not appear to go to zero as $t \to \infty$ as linear theory predicts.

Comparisons with the experimental results of Baines (1979) for very small-amplitude obstacles were also done. For this purpose Baines' obstacle M2 with a non-dimensional amplitude of 0.059 was used. The numerical results agreed well in some aspects when the obstacle profile was modified by adding a boundary layer which retained a constant thickness downstream of the obstacle. Specifically, a flat region of negative U_1 (defined in (3.1 *a*)) near the obstacle is seen at $t = 26.42$, with similar magnitudes and length in the experiments and numerical simulations. These flat regions are transient in the numerical simulations. The position of the wave front upstream of the obstacle is identical in the numerical results and in linear theory. The wave front in the experiments is delayed significantly for some unknown reason (presumably a viscous phenomenon).

One long-time run was done. Following a transient startup period, with large-amplitude oscillations, a periodic state with small non-decaying oscillations about Long's model solution was reached. In contrast, the experimental results of Baines (1977) showed poor agreement with Long's model. This is believed to be due to viscous effects, in particular boundary-layer separation and a wake, which results in the generation of an upstream-propagating disturbance. The numerical results also suggest that the experimental observations were taken during the initial transient period of large-amplitude oscillations, before a final steady state was achieved. The implication of this run is that idealized inviscid flow approaches a state comprised of small oscillations about Long's model solutions, provided that breaking has not occurred in the transient phase.

An investigation into the obstacle amplitudes required for breaking was also done. It was found that transient breaking generally occurred for amplitudes well below the value predicted by Long's model due to the generation of very large transient mode-one waves downstream of the obstacle. For large-amplitude obstacles breaking first occurred at the top of the domain slightly downstream from the obstacle. At later times, it occurred farther and farther downstream at locations alternating between the bottom and top of the domain. As the obstacle amplitude was decreased the strength of the first breaking event decreased and ultimately disappeared. The strengths of the subsequent breaking events also decreased but more slowly so they could be stronger than the first breaking event. Breaking at a given location may occur repeatedly due to an oscillating attached lee wave. For F close to 0.5 the behaviour is qualitatively different. Breaking occurs for obstacle amplitudes larger than the breaking amplitude predicted by Long's model only after a long time, due to a slowly strengthening mode-two wave above the obstacle. These results agree with experimental observations (Baines 1977) which showed wave breaking for obstacles amplitudes well below those predicted by Long's model except for F^{-1} close to integer values.

The large-amplitude transient waves which resulted in wave breaking are mode-one waves with an upstream phase velocity and a downstream group velocity. As F decreases, their wavelength and amplitude decreases. A dominant wavelength does not exist if F is much smaller that $\frac{2}{3}$.

Immediately downstream of the obstacle there is a lee wave attached to the obstacle with a periodically varying amplitude. As its amplitude decays (i.e. U_1 decreases) a

mode-one wave of positive U_1 leaves the obstacle to propagate upstream. At the same time a mode-two wave with a negative value of U_2 leaves the obstacle. It propagates against the flow while being advected downstream. This process repeats periodically. Wave breaking occurs near the top of the domain just downstream of the obstacle when U_1 is sufficiently large. If breaking does not occur in the first cycle it may occur in subsequent ones as the peak amplitude of the attached lee wave may grow over several cycles before decaying.

The wave drag oscillates with the attached lee wave. The wave drag period is independent of the obstacle amplitude and varies with $K = F^{-1}$, increasing from about 10 to infinity as K decreases from 2 to 1. The values agree quite well with the experimental results of Castro *et al.* (1990) for $K \geqslant 1.5$. In both the numerical and experimental results the amplitude of the oscillations does not appear to decay with time. For $K < 1.5$ the experimental results showed no oscillations in the wave drag. These experiments used bluff obstacles, including a two-dimensional fence and a very narrow Witch of Agnesi profile, for which there was flow separation in the obstacle lee. This makes the similarity of the numerical and experimental results all the more striking. In the experiments with $K < 1.5$ the longer-period oscillations may have been damped out by turbulent mixing in the wake.

Castro *et al.* (1990) discussed possible mechanisms for the cause of the periodic oscillations of the wave drag. One suggestion was that the variations in wave drag were a consequence of variations of the effective value of K upstream of the obstacle. In their experiments, significant upstream columnar disturbances were generated. For $K > 1.5$ the amplitude, A, of the columnar disturbance decreases with K. An oscillation sets in, as the presence of a columnar disturbance implies an increase in the wave propagation speed which increases the effective value of K. This decreases A, which in turn reduces the effective value of K; A then increases again. This gives rise to periodic variations in the strength of the columnar disturbance and of the wave drag.

In the current inviscid simulations there are no columnar disturbances which permanently modify the upstream flow conditions. In the light of these inviscid calculations, a more appropriate interpretation of Castro *et al.*'s results is that suggested by Baines (1994). An upstream columnar disturbance is generated because of the momentum source associated with the wake attached to the lee of the obstacle. Oscillations of the wave drag are due to waves superimposed on the columnar disturbance.

Another possible mechanism suggested by Castro *et al.* (1990) was that it is a nonlinear process governed by a forced KdV-type equation. They discarded this possibility because the theoretical work of Grimshaw & Smyth (1986) showed that for uniform stratification the nonlinear self-interaction term vanishes. Grimshaw & Yi (1991, GY) have since derived a new KdV-type nonlinear evolution equation for near-resonant flow (i.e. $F \approx 1/n$) in the weakly stratified ($\approx$ Boussinesq) limit which describes several features of the numerical simulations. Specifically: (i) for slightly subcritical flow (i.e. F slightly less than 1) it predicts breaking lee waves for obstacle amplitudes above the hydrostatic breaking amplitude; (ii) solutions have lee waves with an upstream phase velocity; (iii) the emergence of upstream-propagating waves appears to be coupled with the collapse of a large lee wave just downstream of the obstacle. Thus, GY's equation describes some of the salient features of the evolution of the mode-one wave seen in these numerical solutions for cases which are far from resonance, have narrow obstacles, and are strongly nonlinear. The similarity with GY's solutions improves as $F \to 1$. The numerical result that the behaviour is different near $F = 0.5$ may appropriately be viewed as F being farther from resonance ($F = 1$) rather

than close to 0.5. The mode-two waves may be a result of the interaction of the mode-one waves with the obstacle and of the self-interaction of the mode-one waves. They act to inhibit breaking and may partially account for the longer breaking times obtained in the model results, which are about two to three times longer than predicted by GY. Another possible explanation for the earlier breaking found by GY is that their theory is in the wide-obstacle limit. Model results indicate that breaking occurs more rapidly as the obstacle width is increased.

This work was funded by grants from the Natural Sciences and Engineering Research Council of Canada and the Canadian Department of Fisheries and Oceans.

REFERENCES

BAINES, P. G. 1977 Upstream influence and Long's model in stratified flows. *J. Fluid Mech.* **82**, 147–159.

BAINES, P. G. 1979 Observations of stratified flow over two-dimensional obstacles in fluid of finite depth. *Tellus* **31**, 351–371.

BAINES, P. G. 1994 *Topographic Effects in Stratified Flows*. Cambridge University Press (to appear).

BELL, J. B., COLELLA, P. & GLAZ, H. M. 1989*a* A second-order projection method for the incompressible Navier–Stokes equations. *J. Comput. Phys.* **85**, 257–283.

BELL, J. B. & MARCUS, D. L. 1992 A second-order projection method for variable-density flows. *J. Comput. Phys.* **101**, 334–348.

BELL, J. B., SOLOMON, J. M. & SZYMCZAK, W. G. 1989*b* A second-order projection method for the incompressible Navier Stokes equations on quadrilateral grids. *AIAA 9th Computational Fluids Dynamics Conf., Buffalo, NY, June 14–16, 1989.*

BENJAMIN, T. B. 1970 Upstream influence. *J. Fluid Mech.* **40**, 49–79.

BOYER, D. L. & TAO, L. 1987 Impulsively started, linearly stratified flow over long ridges. *J. Atmos. Sci.* **44**, 23–42.

CASTRO, I. P. 1994 Effects of stratification on separated wakes: Part I. Weak static stability. *Proc. 3rd IMA Meeting on Stably Stratified Flows (Leeds, 1989)* (to appear).

CASTRO, I. P. & SNYDER, W. H. 1988 Upstream motions in stratified flow. *J. Fluid Mech.* **187**, 487–506.

CASTRO, I. P. & SNYDER, W. H. 1990 Obstacle drag in stratified flow. *Proc. R. Soc. Lond.* A **429**, 119–140.

DAVIS, R. E. 1969 The two-dimensional flow of a stratified fluid over an obstacle. *J. Fluid Mech.* **36**, 127–143.

GOLUB, G. H. & VAN LOAN, C. F. 1989 *Matrix Computations*, 2nd edn, pp. 170–171. The Johns Hopkins University Press.

GRIMSHAW, F. & SMYTH, N. 1986 Resonant flow of a stratified fluid over topography. *J. Fluid Mech.* **169**, 429–464.

GRIMSHAW, R. & YI, Z. 1991 Resonant generation of finite-amplitude waves by the flow of a uniformly stratified fluid over topography. *J. Fluid Mech.* **229**, 603–623 (referred to herein as GY).

HANAZAKI, H. 1989 Upstream advancing columnar disturbances in two-dimensional stratified flow of finite depth. *Phys. Fluids* A **1**, 1976–1987.

HANAZAKI, H. 1992 A numerical study of nonlinear waves in a transcritical flow of stratified fluid past an obstacle. *Phys. Fluids* A **4**, 2230–2243.

HANAZAKI, H. 1993 On the nonlinear internal waves excited in the flow of a linearly stratified Boussinesq fluid. *Phys. Fluids* A **5**, 1201–1205.

JANOWITZ, G. S. 1981 Stratified flow over a bounded obstacle in a channel of finite height. *J. Fluid Mech.* **110**, 161–170.

LONG, R. R. 1953 Some aspects of the flow of stratified fluids. I. A theoretical investigation. *Tellus* **5**, 42–58.

LONG, R. R. 1955 Some aspects of the flow of stratified fluids. III. Continuous density gradients. *Tellus* **7**, 341–357.

LONG, R. R. 1972 Finite amplitude disturbances in the flow of inviscid rotating and stratified fluids over obstacles. *Ann. Rev. Fluid Mech.* **4**, 69–92.

MCINTYRE, M. E. 1972 On Long's hypothesis of no upstream influence in uniformly stratified or rotating flow. *J. Fluid Mech.* **52**, 209–243.

WEI, S. N., KAO, T. W. & PAO, H.-P. 1975 Experimental study of upstream influence in the two-dimensional flow of a stratified fluid over an obstacle. *Geophys. Fluid Dyn.* **6**, 315–336.